Remote Sensing of Environment 298 (2023) 113812

Contents lists available at ScienceDirect

Remote Sensing of Environment

journal homepage: www.elsevier.com/locate/rse

DiluviumDEM: Enhanced accuracy in global coastal digital elevation models

Dominick Dusseau *, Zachary Zobel, Christopher R. Schwalm

Woodwell Climate Research Center, 149 Woods Hole Rd, Falmouth, MA 02540, USA

ARTICLE INFO

Edited by Menghua Wang

Keywords:
Digital elevation model
LightGBM
Sea level rise
Global

ABSTRACT

Accurate representation of global coastal topography is essential for numerous scientific disciplines, coastal management, and disaster risk assessment. Even with recent improvements to existing global digital elevation models (DEMs), high and persistent errors in these DEMs result in significant uncertainty when analyzing coastal processes. This results in low confidence for current sea level rise inundation risk assessments. We present DiluviumDEM, the first global DEM appropriate (i.e., the root mean square error (RMSE) is half the total water elevation in 2100 under a specific scenario) for mapping sea level rise inundation under the IPCC SSP2–4.5 and SSP5–8.5 scenarios, with an estimated RMSE of 1.13 m for coastal areas with elevations less than 2 m above mean sea level. Out of ten countries used for validation, DiluviumDEM has the lowest RMSE compared to three other DEMs analyzed, the lowest mean absolute error (MAE) for eight, and the mean error (ME) closest to zero for six. By reducing the error of the European Space Agency's Copernicus DEM using a gradient boosted decision tree model, we have created a new global coastal DEM with up to twice the accuracy compared to other global DEMs.

1. Introduction

Global coastal digital elevation models (DEMs) are crucial in a wide range of applications, including hydrological modeling, hazard risk assessment, and land use planning. One important application for coastal DEMs is sea level rise inundation mapping. Accurate projections of land inundated due to sea level rise are necessary for adaptation and risk management planning. However, despite significant advancements in processing techniques, errors inherent in DEMs persist and can significantly impact the reliability and accuracy of derived analyses and decision-making processes. Root mean square error (RMSE) is a common metric for assessing the accuracy of DEMs and represents the distribution of errors within a DEM (Gesch, 2018). Technology such as Light Detection and Ranging (LiDAR) can generate DEMs with extremely low errors, generally between 15 cm and 50 cm RMSE (ICSM, 2008). While using DEMs derived from LiDAR is optimal, such DEMs are not available globally due to the high costs associated with taking LiDAR surveys and because many governments do not make LiDAR DEMs publicly available. Private sector involvement, such as the insurance sector, in creating a global LiDAR dataset would be ideal given the importance of elevation data in flood insurance contexts. Continental and global analyses must rely on satellite-derived DEMs such as the Shuttle Radar Topography Mission (SRTM) (Rabus et al., 2003), NASADEM (Crippen et al., 2016), ALOS World 3D – 30 m (AW3D30) (Tadono et al., 2014), and Copernicus DEM (referred to as COP30DEM) (ESA, 2021). The errors associated with these DEMs vary across data products and spatially. SRTM, a highly popular global DEM due to its accessibility, has a RMSE of 7.16 m and AW3D30 has a RMSE of 6.82 m among elevations lower than 20 m in Hispaniola (Zhang et al., 2019). In Massachusetts, USA, SRTM has a RMSE of almost 10 m (Farr et al., 2007). A comparison completed in the Philippines showed AW3D30 to be considerably more accurate than SRTM with respective RMSEs of 5.68 m and 8.28 m (Santillan and Makinano-Santillan, 2016). One of the more recently released global DEMs, COP30DEM, shows greater accuracy compared to older DEMs. Guth and Geoffroy (2021) found that COP30DEM represented terrain elevations better than SRTM, NASADEM, and AW3D30. Gesch (2018) found that in areas less than or equal to 10-m elevation for the continental United States, NASADEM and AW3D30 have a RMSE of 3.10 and 3.12 m, respectively, which outperform SRTM which has a RMSE of 4.55 m. The Forest And Buildings removed DEM (FABDEM) has been shown to be the most accurate DEM in the continental coastal zone of the United States with a RMSE of 1.23 m (Gesch, 2023).

* Corresponding author.
E-mail addresses: ddusseau@woodwellclimate.org (D. Dusseau), zzobel@woodwellclimate.org (Z. Zobel), cschwalm@woodwellclimate.org (C.R. Schwalm).

https://doi.org/10.1016/j.rse.2023.113812
Received 5 January 2023; Received in revised form 17 August 2023; Accepted 6 September 2023
Available online 18 September 2023

Such high errors have important implications for sea level rise studies and planning because the RMSE of DEMs is often double or triple, if not more, the amount of sea level rise anticipated by 2100. The high uncertainty surrounding the sea level rise inundation extent maps is a serious limitation that hampers policy making decisions in areas where LiDAR data is not available. Various users from scientists to geospatial analysts are forced to use low-confidence sea level rise inundation risk data which can bias estimates of population exposure to coastal flooding. Many previous analyses have worked to correct DEM errors originating from, for example, dense tree canopies (satellite radar generally cannot fully penetrate vegetation and reach the ground), building height (satellite sensors generally capture the elevation of the top of the building rather than the ground), slope (higher slope is correlated with higher errors), and instrument alignment (Hawker et al., 2019; Hawker et al., 2022; Khasanov, 2020; Li et al., 2022). Work by Kulp and Strauss (2018, 2021) resulted in CoastalDEMV2.1, a DEM focused on coastal areas whereby a neural network was used to globally correct NASADEM. The most recent advance has been from Hawker et al. (2022) where a correction algorithm was used to globally correct the COP30DEM for building and forest elevation errors resulting in FABDEM.

Here, we present a next generation global coastal DEM, DiluviumDEM (Latin for 'flood'), with reduced vertical error that can be used for a variety of applications including flood modeling, sea level rise inundation mapping, and other coastal processes. Elevation error is reduced by using a gradient boosted decision tree model to correct COP30DEM.

2. Methods

DiluviumDEM is a global DEM for coastal areas and is publicly available for any use. DiluviumDEM was created by estimating the elevation error in COP30DEM for each pixel using the gradient boosted decision trees regression model, LightGBM, and then subtracting the predicted error from COP30DEM (ESA, 2021; Ke et al., 2017). Other well-known implementations of gradient boosted decision trees are XGBoost and pGBRT (Chen and Guestrin, 2016; Tyree et al., 2011). LightGBM was chosen due to two improvements in the algorithm: Gradient-based One-Side Sampling and Exclusive Feature Bundling. These refinements allow LightGBM to achieve very similar accuracies as traditional gradient boosted decision trees but with a significant decrease in computation time (Ke et al., 2017). To the best of our knowledge, this is the first use case of LightGBM to correct vertical errors in a DEM. LightGBM, a popular machine learning algorithm, holds some similarities to Random Forest models which are widely utilized in remote sensing applications (Belgiu and Drăguţ, 2016). However, there are key differences between the two:

1) The model architecture differs in that LightGBM uses an ensemble of weak decision trees built sequentially, enhancing the correction of errors made by the previous trees. LightGBM focuses on the nodes that obtain the greatest loss reduction using a leaf-wise tree growth framework. Random Forests create an ensemble of independent decision trees using a random subset of training features and samples and then aggregating the final predictions of all trees.
2) The gradient boosting approach of LightGBM optimizes a loss function by tuning model parameters during training. Random Forests train each tree independently with random training samples.
3) Random Forests are usually slower than LightGBM because LightGBM uses a leaf-growth strategy and histogram-binning method while Random Forests creates each tree independently which increases computation time.
4) Random Forests have better interpretability because feature importance can be understood through individual decision trees while LightGBM's sequential tree construction adds complexity when analyzing feature importance.

LightGBM lends itself to global DEM correction due to the large datasets utilized. Initial testing against a neural network revealed that LightGBM was superior in reducing DEM vertical error. Due to limited time available for model testing, a Random Forest model was evaluated. Although it is beyond the scope of this study to determine the preferable model architecture for corrected DEMs, LightGBM's regression framework demonstrates strong applicability for remote sensing use cases (Pham et al., 2020).

COP30DEM was chosen because (1) it is licensed for any use, (2) does not suffer from the stripe noise that is common in SRTM data, (3) has been smoothed for noise which enhances the elevation signal, (4) the data was gathered from 2011 to 2015; more recent than the SRTM data from 2000, and (5) COP30DEM uses the geoid EGM2008 as the vertical datum which is three to six times as accurate as EGM96, the geoid and datum for SRTM/NASADEM (Fahrland et al., 2022; Gallant and Read, 2009; Pavlis et al., 2012). Two DEMs were used as the ground truth elevations to train the model and evaluate performance. The first is the NOAA Sea Level Rise Viewer DEM (available at https://coast.noaa.gov/htdata/raster2/elevation/SLR_viewer_DEM_6230/). DEMs for all coastal states of the continental United States were used. The LiDAR used to create the NOAA DEMs were acquired between 1996 and 2016 with most being acquired in the 21st century. Most of the NOAA SLR DEMs have a RMSE less than 20 cm (NOAA, 2012). The second DEM used for training is the Actueel Hoogtebestand Nederland Version 2 (AHN2) (https://www.ahn.nl/). The LiDAR data used to create the AHN2 was taken between 2007 and 2012 and the AHN2 has a RMSE of 10 cm. All data points in NOAA DEMs and the AHN2 DEM were used for either training or validation. The NOAA DEM data was converted from NAVD88 to EGM2008 using the NOAA VDatum software. The AHN2 data was converted from the vertical datum NAP to EGM2008 using the RDNAPTRANS2018 parameters (https://www.nsgi.nl/rdnaptrans) (Lesparre et al., 2020). The ground-truth data was split 70% for training and 30% for validation. This resulted in approximately 252 million pixels used for training and 108 million pixels used for validation in the continental United States. In the Netherlands, approximately 39 million pixels and 16 million pixels were used for training and validation, respectively. The training and validation data are first separated by converting from Geotiffs to randomly shuffled TFRecord files each containing data for 10,000 pixels. The TFRecord files are then randomly shuffled before model training begins. This two-step data shuffling process promotes model generalization and allows for a randomly spatially distributed training and validation dataset instead of training and validating on specific regions.

The error between COP30DEM and the LiDAR-derived DEMs is calculated for each pixel and then used as the ground truth data for LightGBM. All pixels between the elevation band of −10 and 80 m were selected for correction and any pixels marked as water by the COP30-DEM water mask were removed from the selection. Pixels in this elevation range were chosen for several reasons. First, the model's focus was primarily on coastal areas, which justified prioritizing elevations in that range. Second, incorporating negative elevations down to −10 m helped address any potential negative biases present in the COP30DEM data. Third, an upper bound of 80 m was set to rectify significant positive biases that could arise from tall buildings. However, it's important to note that due to this upper range limitation, there might be a noticeable step change of a few meters at the 80-m elevation threshold when comparing DiluviumDEM to COP30DEM. DiluviumDEM is meant for coastal applications; for use cases focusing in areas with elevations greater than 80 m, i.e., not on sea level rise, we suggest utilizing other DEMs.

To deal with potential errors in DiliuviumDEM arising from the tidal extent ranging across the explanatory variables' collection time periods, we use the COP30DEM water body mask, which is based on data from WorldDEM, that represents the high-water mark globally (Fahrland et al., 2022; Airbus, 2018). Therefore, the greatest permanent water extent has been considered when applying a final water mask to

DiluviumDEM. Also, we use the Dynamic World Flooded Vegetation Areas dataset as an input variable into the model to account for pixels that are temporarily flooded by tides. This would allow the model to recognize wetland areas during training.

The Google Earth Engine platform was used to combine and export all training and prediction data (Gorelick et al., 2017). A total of 52 explanatory variables were used to predict the COP30DEM error. They include vegetation cover, canopy height, satellite LiDAR, population density, land and cover. A complete inventory of variables used to develop DiluviumDEM is presented in the supplemental materials. All input variables were resampled at a 30-m resolution and aligned to the COP30DEM grid in Google Earth Engine to compute the pixel-by-pixel error. Similar resampling and georeferencing was done for creating CoastalDEM and FABDEM (Hawker et al., 2022; Kulp and Strauss, 2018). A small selection of pixels in the elevation band −10 m to 80 m were not corrected because either Landsat or Sentinel 2 data was not available. The areas where pixels were not corrected is largely limited to coastal areas with steep topography such as northern Chile where inundation risk is negligible.

To show the accuracy of DiluviumDEM, we compare the RMSE, mean absolute error (MAE), and the mean error (ME) of the elevation model to FABDEM, COP30DEM, and CoastalDEMV2.1. While FABDEM and COP30DEM are not coastal DEMs, they are recent advances in global DEMs and are valuable comparisons to DiluviumDEM. Data from eight countries (USA, the Netherlands, Australia, England, Poland, Japan, France, Mexico, Latvia, and Denmark) with LiDAR-based DEMs was used as validation. All LiDAR-based DEMs have a RMSE of 30 cm or less. All country LiDAR datasets were converted from their respective datums to EGM2008 using geoids for each country and dataset. Additional validation of DiluviumDEM was completed with the ATLAs/ICESat2 L3A Land and Vegetation Height, Version 5 (ATL08) ground elevation points from October 14, 2018 to December 22, 2021. The preprocessing steps to clean the ground track data and convert the elevation values to the EGM08 datum were taken from Vernimmen et al. (2020).

In order to determine the value of using DiluviumDEM versus other DEMs for inundation mapping and modeling, error metrics (e.g., RMSE) must be translated to a confidence level for a particular water elevation. Another way to describe the confidence level is the degree to which the areas estimated as inundated are accuracy mapped as such. Gesch (2018) describes this method in detail and derives the confidence interval from the standard deviation of the errors of a normal distribution assuming a mean value of zero (also known as an unbiased normal distribution). Assuming the DEMs are unbiased (e.g., a mean error of zero), we can then substitute the standard deviation used for calculating the confidence interval for the RMSE (Woodruff and BenDor, 2018). NOAA (2010) describes a DEM as appropriate for a particular water elevation if the RMSE of the DEM is half of the water elevation. In the methodology of Gesch (2018), a RMSE that is half of the water level would be a confidence level of 68% and we apply this definition here. This method assumes the use of a bathtub inundation model. We note that the criteria for appropriateness would change if a more advanced hydrodynamic model is implemented as this would also change the extent of inundation. We use the bathtub model assumption because determining hydrologic connectivity is computationally expensive at this geographic scale and the bathtub model is a conservative estimate of areas vulnerable to sea level rise inundation. The vertical reference for CoastalDEMV2.1 was converted to EGM2008 using the EGM96 and EGM2008 geoids from Agisoft (https://www.agisoft.com/downloads/geoids/).

For any country-level spatial aggregation completed, the Exclusive Economic Zones (EEZ) from Flanders Marine Institute (2020) were used as administrative boundaries rather than country polygons because the boundaries representing the coastlines are often imperfect. For spatial aggregations at the Level 1 administrative unit scale (e.g., provinces and states), the GADM (Database of Global Administrative Areas) dataset is used (https://gadm.org).

3. Results

3.1. Statistical comparison

DiluviumDEM is the best-in-class global coastal DEM since it shows the greatest accuracy across most metrics. In the instances where other DEMs have lower errors, DiluviumDEM has very similar error magnitudes, usually a difference of less than 10 cm relative to 0.77 m of sea level rise by 2100 under the SSP5–8.5 Medium Confidence scenario. Out of the 90 individual comparisons (across countries, elevation thresholds, and error metrics), DiluviumDEM shows the lowest error for 70, FABDEM for 14, and CoastalDEMV2.1 for 6. Tables 1, 2, and 3 show the RMSE, MAE, and ME, respectively, for each DEM. While ME is useful for understanding the overall bias of a DEM, large positive and negative errors can cancel out leading to a low ME but would also result in a high RMSE. Therefore, it is important to compare DEMs holistically across metrics and not in isolation to avoid misinterpreting a DEM's accuracy. The statistics shown for the USA and the Netherlands only include pixels that were used for validation, not training. We focus on the elevation thresholds of 2 and 5 m because these are the coastal regions that will be impacted by sea level rise through 2100. We also include the elevation threshold of 10 m as these areas are vulnerable to storm surge.

DiluviumDEM maintains the lowest MAE and RMSE across all countries compared to the other DEMs except for the MAE value of Denmark and England. DiluviumDEM exhibits the ME closest to zero for most countries. For those four countries where DiluviumDEM is not superior – having error metrics closest to zero for 2 or more of the elevation thresholds – the ME of DilviumDEM is only, on average, 8 cm further from zero than the leading DEM. We emphasize that the ME of DiluviumDEM is more consistently close to zero across the countries compared to the other global DEMs. Moreover, the improvement compared to other DEMs is significant. The RMSE of DiluviumDEM is below 2 m for all countries and less than 1.5 m for eight out of the ten nations analyzed. DiluviumDEM has an RMSE that is more than half a meter less than the FABDEM's RMSE for seven out of the ten countries. Skill relative to CoastalDEMV2.1 is even better—DiluviumDEM's RMSE is more than a meter less than CoastalDEMV2.1's for 6 countries and more than half a meter less for all countries. Not only does DiluviumDEM consistently show the lowest composite error metrics for all regions, but DiluviumDEM provides a substantial improvement in estimating coastal elevations over other publicly available global DEMs.

Both FABDEM and DiluviumDEM were trained with Netherlands LiDAR data, yet DiluviumDEM has lower out-of-sample error metrics than FABDEM in this region. Only FABDEM was trained with data from Latvia and Australia yet DiluviumDEM outperforms FABDEM in both countries in the coastal lowlands. This out-of-sample superiority underscores the ability to use DiluviumDEM in locations where training data was not used. An additional finding is that, based on the RMSE and MAE metrics, FABDEM is superior to CoastalDEMV2.1 in seven of the countries analyzed even though CoastalDEMV2.1 was designed for coastal areas.

To determine how DiluviumDEM performs for different land covers and provide guidance for users, we calculated RMSE, MAE, and ME for the built area and tree land covers using the ESRI 2020 Global Land Use Land Cover from Sentinel-2 (Karra et al., 2021). Tables 3 and 4 show the error metrics across countries for the built area and tree land covers, respectively. Within the built area, DilivumDEM also outperforms the other global DEMs. For 7 out of the 10 countries assessed, DilivumDEM shows higher accuracy for all three metrics. In England, FABDEM contains the ME and MAE closest to zero while DiluviumDEM has the lowest RMSE. FABDEM also shows the lowest MAE in Denmark and ME closest to zero in Japan with DilivumDEM having the values closest to zero for the other two metrics for the respective countries. DilivumDEM performs similarly in the tree land cover. DiliviumDEM maintains the superior ME, RMSE, and MAE in all countries except for the ME in Denmark, Latvia, Mexico, England, and USA where CoastalDEMV2.1 is

Table 1
RMSE in meters for different global DEMs using an airborne LiDAR-based DEM as the reference dataset. Only pixels with elevations greater than zero and less than the elevation threshold, according to both the LiDAR or the global DEM, were used. The value closest to zero of each row is in bold. Country abbreviations are USA: Continental United States, NLD: the Netherlands, AUS: Australia.

Country	Elevation Threshold (m)	DiluviumDEM	FABDEM	COP30DEM	CoastalDEMV2.1 (90 m)
USA	2	**0.85**	2.58	5.92	1.96
	5	**1.03**	2.85	6.56	2.25
	10	**1.15**	3.00	6.81	2.50
NLD	2	**0.68**	0.96	2.14	1.28
	5	**0.74**	1.10	1.04	1.44
	10	**0.77**	1.17	3.35	1.56
AUS	2	**1.60**	2.57	4.41	3.35
	5	**1.61**	2.32	4.25	3.12
	10	**1.78**	2.34	4.45	3.56
England	2	**0.95**	1.20	1.46	2.21
	5	**1.03**	1.36	1.83	2.43
	10	**1.16**	1.54	2.25	2.54
Poland	2	**0.97**	1.74	4.34	1.36
	5	**1.20**	2.00	5.09	1.74
	10	**1.44**	2.25	5.82	2.07
Japan	2	**1.66**	2.48	2.45	5.15
	5	**1.67**	2.33	2.83	5.04
	10	**1.87**	2.49	3.14	5.36
France	2	**0.99**	1.70	2.09	2.31
	5	**1.13**	1.85	2.63	2.58
	10	**1.34**	2.05	3.11	2.81
Mexico	2	**1.03**	1.50	2.66	1.75
	5	**1.12**	1.66	2.79	2.03
	10	**1.21**	1.81	3.06	2.26
Latvia	2	**1.38**	1.74	5.28	1.59
	5	**1.65**	2.46	7.95	2.06
	10	**1.79**	2.55	8.97	2.41
Denmark	2	**1.13**	1.21	2.29	1.65
	5	**1.31**	1.48	3.05	1.86
	10	**1.39**	1.63	3.41	1.99

Table 2
MAE in meters for different global DEMs using an airborne LiDAR-based DEM as the reference dataset. Only pixels with elevations greater than zero and less than the elevation threshold, according to both the LiDAR or the global DEM, were used. The value closest to zero of each row is in bold. Country abbreviations are USA: Continental United States, NLD: the Netherlands, AUS: Australia.

Country	Elevation Threshold (m)	DiluviumDEM	FABDEM	COP30DEM	CoastalDEMV2.1 (90 m)
USA	2	**0.51**	1.37	3.21	1.24
	5	**0.63**	1.57	3.85	1.44
	10	**0.70**	1.67	4.16	1.62
NLD	2	**0.41**	0.51	1.07	0.91
	5	**0.44**	0.57	1.36	0.99
	10	**0.46**	0.59	1.65	1.07
AUS	2	**0.95**	1.43	2.30	2.04
	5	**0.97**	1.33	2.29	1.91
	10	**1.04**	1.33	2.40	2.25
England	2	0.60	**0.48**	0.64	1.04
	5	0.61	**0.55**	0.79	1.20
	10	0.65	**0.64**	0.96	1.33
Poland	2	**0.61**	0.82	1.92	0.81
	5	**0.68**	0.97	2.41	1.02
	10	**0.78**	1.12	2.85	1.26
Japan	2	**0.75**	0.85	1.12	2.21
	5	**0.81**	0.90	1.41	2.31
	10	**0.89**	1.01	1.53	2.59
France	2	**0.50**	0.57	0.83	1.00
	5	**0.57**	0.72	1.15	1.21
	10	**0.68**	0.88	1.44	1.41
Mexico	2	**0.68**	0.98	1.45	1.34
	5	**0.74**	1.10	1.62	1.47
	10	**0.79**	1.19	1.85	1.57
Latvia	2	**0.86**	0.95	2.57	1.11
	5	**1.04**	1.38	4.61	1.45
	10	**1.16**	1.51	5.70	1.75
Denmark	2	0.71	**0.57**	0.94	0.94
	5	0.82	**0.69**	1.29	1.09
	10	0.86	**0.78**	1.48	1.22

Table 3
ME in meters for different global DEMs using an airborne LiDAR-based DEM as the reference dataset. Only pixels with elevations greater than zero and less than the elevation threshold, according to both the LiDAR or the global DEM, were used. The value closet to zero of each row is in bold. Country abbreviations are USA: Continental United States, NLD: the Netherlands, AUS: Australia.

Country	Elevation Threshold (m)	DiluviumDEM	FABDEM	COP30DEM	CoastalDEMV2.1 (90 m)
USA	2	**0.08**	0.67	2.94	0.38
	5	0.06	0.82	3.64	**0.05**
	10	**0.03**	0.87	3.97	−0.18
NLD	2	**0.01**	0.05	0.74	−0.45
	5	**−0.01**	0.10	1.04	−0.52
	10	**−0.02**	0.13	1.33	−0.59
AUS	2	**0.16**	0.82	1.67	0.35
	5	**0.12**	0.67	1.71	−0.27
	10	**0.11**	0.62	1.88	−0.82
England	2	0.06	**−0.01**	0.15	−0.62
	5	**0.01**	0.05	0.33	−0.90
	10	**−0.01**	0.14	0.53	−0.84
Poland	2	0.30	0.69	1.82	**−0.09**
	5	0.22	0.81	2.30	**−0.16**
	10	**0.16**	0.90	2.73	−0.29
Japan	2	−0.21	**0.01**	0.59	−1.01
	5	−0.17	**0.11**	0.96	−1.45
	10	−0.20	**0.15**	1.07	−1.77
France	2	**0.19**	0.24	0.50	−0.61
	5	**0.17**	0.35	0.84	−0.66
	10	**0.14**	0.43	1.12	−0.70
Mexico	2	**0.24**	0.76	1.20	0.71
	5	**0.21**	0.84	1.35	0.43
	10	0.18	0.89	1.59	**0.08**
Latvia	2	−0.32	**0.29**	2.26	−0.50
	5	−0.39	0.75	4.37	**−0.32**
	10	−0.48	0.91	5.51	**−0.33**
Denmark	2	−0.21	**0.18**	0.53	−0.22
	5	−0.32	**0.28**	0.90	−0.27
	10	−0.37	**0.28**	1.08	−0.31

Table 4
RMSE, MAE, and ME for built area land covers. Only pixels with elevations greater than zero and less than 10 m, according to both the LiDAR or the global DEM, were used. The closest to zero of each row is in bold. Country abbreviations are USA: Continental United States, NLD: the Netherlands, AUS: Australia.

Country	Error Metric	DiluviumDEM	FABDEM	COP30DEM	CoastalDEMV2.1 (90 m)
USA	ME	**0.03**	0.88	2.66	−0.38
	MAE	**0.76**	1.21	2.82	1.55
	RMSE	**1.15**	1.98	4.32	2.32
NLD	ME	**−0.03**	0.17	1.87	−0.42
	MAE	**0.66**	0.76	2.06	1.11
	RMSE	**0.97**	1.20	2.98	1.62
AUS	ME	**0.04**	0.61	1.75	−1.12
	MAE	**0.98**	1.17	2.04	2.42
	RMSE	**1.52**	1.91	3.16	3.70
England	ME	−0.25	**0.14**	1.38	−1.28
	MAE	0.92	**0.88**	1.64	1.72
	RMSE	**1.42**	1.54	2.60	2.76
Poland	ME	**0.13**	0.54	1.73	−0.70
	MAE	**0.75**	0.91	1.85	1.33
	RMSE	**1.13**	1.48	2.95	2.12
Japan	ME	−0.18	**−0.02**	1.36	−1.25
	MAE	**0.89**	0.91	1.67	2.16
	RMSE	**1.47**	1.73	2.83	3.61
France	ME	**0.12**	0.61	1.52	−1.06
	MAE	**0.85**	1.03	1.76	1.79
	RMSE	**1.37**	1.67	2.74	3.08
Mexico	ME	**−0.06**	0.71	1.92	−0.37
	MAE	**0.86**	1.28	2.11	1.59
	RMSE	**1.22**	1.81	3.02	2.49
Latvia	ME	**−0.07**	0.41	2.06	−0.80
	MAE	**0.83**	0.84	2.22	1.41
	RMSE	**1.22**	1.30	3.56	1.92
Denmark	ME	**−0.26**	0.46	1.57	−0.46
	MAE	0.95	**0.91**	1.79	1.33
	RMSE	**1.38**	1.40	2.68	2.12

closest to zero.

Additional validation in the form of the error histogram is provided in Fig. 1. Histograms of the error for DiluviumDEM, FABDEM, COP30DEM, CoastalDEMV2.1 against the validation data (not training data) with an elevation threshold of 10 m. A random sample of 4893 pixels were selected (the same pixels for all DEMs) across all validation

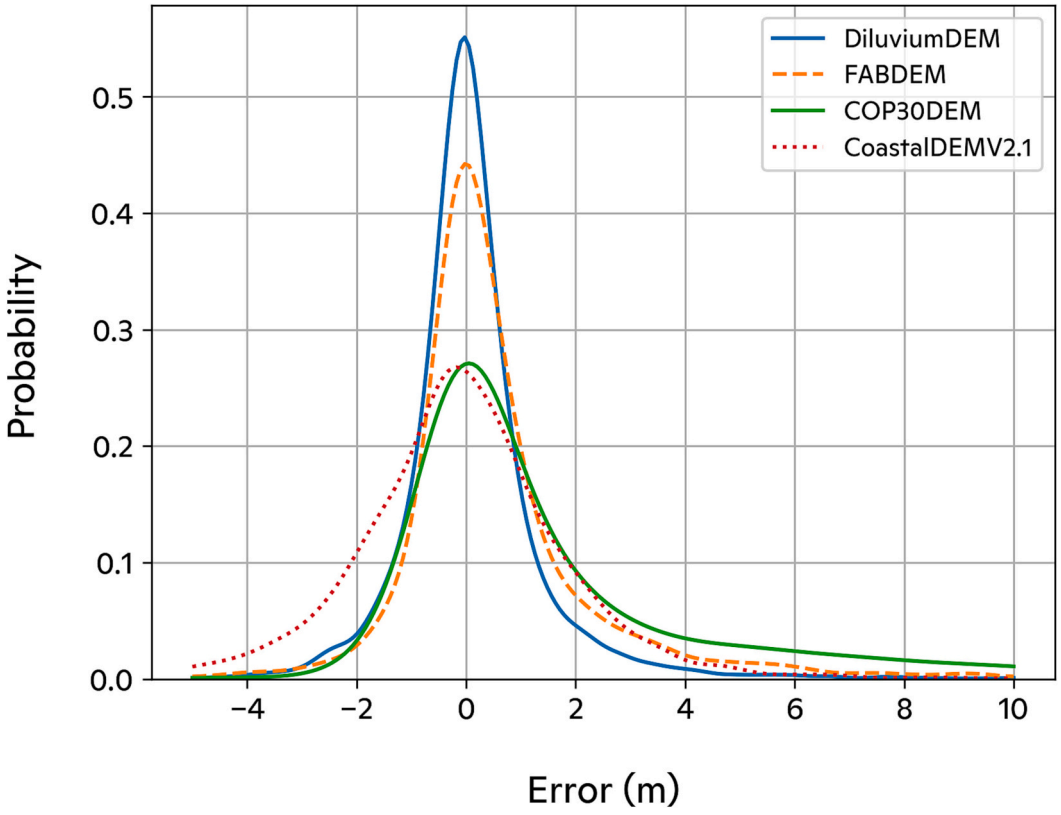

Fig. 1. Histogram comparing DiluviumDEM, FABDEM, COP30DEM, CoastalDEMV2.1 against the validation data (not training data). A random sample of 4893 pixels were selected (the same pixels for all DEMs) across all validation areas with an elevation threshold of 10 m.

Table 5
RMSE, MAE, and ME for tree land covers. Only pixels with elevations greater than zero and less than 10 m, according to both the LiDAR or the global DEM, were used. The value closest to zero of each row is in bold. Country abbreviations are USA: Continental United States, NLD: the Netherlands, AUS: Australia.

Country	Error Metric	DiluviumDEM	FABDEM	COP30DEM	CoastalDEMV2.1 (90 m)
USA	ME	0.07	1.20	7.80	**0.06**
	MAE	**0.99**	2.64	7.84	2.10
	RMSE	**1.47**	3.82	9.92	3.01
NLD	ME	**0.02**	1.47	7.95	0.02
	MAE	**1.03**	1.92	8.01	1.76
	RMSE	**1.45**	2.77	9.61	2.33
AUS	ME	**0.70**	1.74	5.37	−0.37
	MAE	**1.85**	2.45	5.51	2.87
	RMSE	**2.76**	3.52	7.62	4.51
England	ME	0.80	2.87	6.08	**−0.16**
	MAE	**1.87**	3.14	6.26	2.78
	RMSE	**2.70**	3.14	8.29	5.04
Poland	ME	**0.03**	2.64	9.19	−0.22
	MAE	**1.74**	2.93	9.22	2.08
	RMSE	**2.54**	4.10	11.38	3.01
Japan	ME	**−0.19**	2.07	4.85	−9.04
	MAE	**3.08**	3.87	6.07	10.22
	RMSE	**5.34**	6.53	8.75	16.03
France	ME	**0.44**	0.83	4.94	−0.88
	MAE	**1.55**	2.15	5.06	2.46
	RMSE	**2.39**	3.38	7.02	4.18
Mexico	ME	0.38	1.81	3.93	**0.06**
	MAE	**1.26**	2.07	4.01	1.95
	RMSE	**1.76**	2.67	5.09	2.63
Latvia	ME	−0.77	1.58	9.75	**−0.21**
	MAE	**1.65**	2.34	9.83	2.25
	RMSE	**2.25**	3.33	12.09	2.87
Denmark	ME	−0.44	1.78	6.14	**−0.26**
	MAE	**1.79**	2.27	6.24	1.95
	RMSE	**2.52**	3.66	8.61	2.84

areas. All DEMs are centered close to zero; however, DiluviumDEM shows the greatest area under the curve close to zero. The distributions FABDEM and DiluviumDEM have similar peaks, but the FABDEM distribution is flatter as FABDEM contains more positive errors. A comparable assessment applies to COP30DEM but with an even flatter distribution than FABDEM. Finally, the CoastalDEMV2.1 has a similar shape to COP30DEM but is shifted to the left confirming a negative bias in the DEM as shown in Table 3.

The statistics presented in Tables 1 through 5 only account for the elevation uncertainty due to measurement errors. Uncertainty surrounding the vertical datum transformations between the training data datum and the global DEM datum must be accounted for to understand the total error. Since the ICESat2 training elevation data for CoastalDEMV2.1 was transformed from WGS84 to EGM96, the standard deviation included in that conversion is 0.92 m according to VDatum (Kulp and Strauss, 2021; Myers et al., 2007; NOAA, 2021). This is much higher than the standard deviation 0.16 m for converting training elevation data to EGM2008 from NAVD88 which was done for DiluviumDEM (NOAA, 2021). Therefore, the CoastalDEMV2.1 error metrics inherently contain even greater errors.

3.2. Visual comparison

A visual comparison of DEMs also reveals that DiluviumDEM has the lowest errors compared to a reference LiDAR DEM for Tokyo, Japan, Louisiana, USA, and Tabasco, Mexico. In Figs. 2 and 3 we can see the improvements that DiluviumDEM provides in the coastal zone. Fig. 2 shows the elevation range from zero to twenty meters for DiluviumDEM, FABDEM, and the reference LiDAR DEM and Fig. 3 depicts the difference between the global DEMs and the reference LiDAR DEM. In all three areas, DiluviumDEM elevations are very similar to the LiDAR DEM while FABDEM deviates and is mostly greater than the LiDAR elevations. The quality of DiluviumDEM is most pronounced when looking at data in Tabasco, Mexico and Louisiana, USA. Here the DiluviumDEM error is much lower than FABDEM as shown in Fig. 3. To quantify the differences in Fig. 3, the RMSE of DiluviumDEM in Tokyo, Tabasco, and Louisiana is 2.00 m, 0.91 m and 0.60 m, respectively while the RMSE of FABDEM in Tokyo, Tabasco, and Louisiana is 2.42 m, 1.32 m, 2.4 m, respectively for areas less than 2 m above mean sea level. Large portions of those two regions show FABDEM overestimating elevations in the lowlands. FABDEM has pixels in Tabasco and Louisiana that appear close to 20 m within the lowlands area and are largely absent in DiluviumDEM. The differences between DiluviumDEM and the LiDAR DEM are difficult to identify as DiluviumDEM closely resembles the airborne LiDAR data.

The differences between DiluviumDEM and FABDEM are less noticeable in Tokyo, Japan but DiluviumDEM represents elevations that are closer to the reference LiDAR DEM across the coastal lowland as shown in Fig. 3. For many areas in Tokyo, DiluviumDEM is one to two meters less than FABDEM, especially in the northern half of the map. Other parts of the city have even clearer differences such as in the southwest quadrant where a portion of the coastal floodplain is close to zero elevation in the LiDAR DEM, but shows as 5 to 10 m in DiluviumDEM and even higher still in FABDEM. One pattern for DiliviumDEM in Tokyo is slight underestimations of elevation especially in the northern part of the map.

While the low errors of DiluviumDEM in Louisiana are influenced by the machine learning model trained on USA LiDAR data, the low DiluviumDEM errors in Mexico and Japan are an indication of the applicability of DiluviumDEM in areas where the model was not trained. The

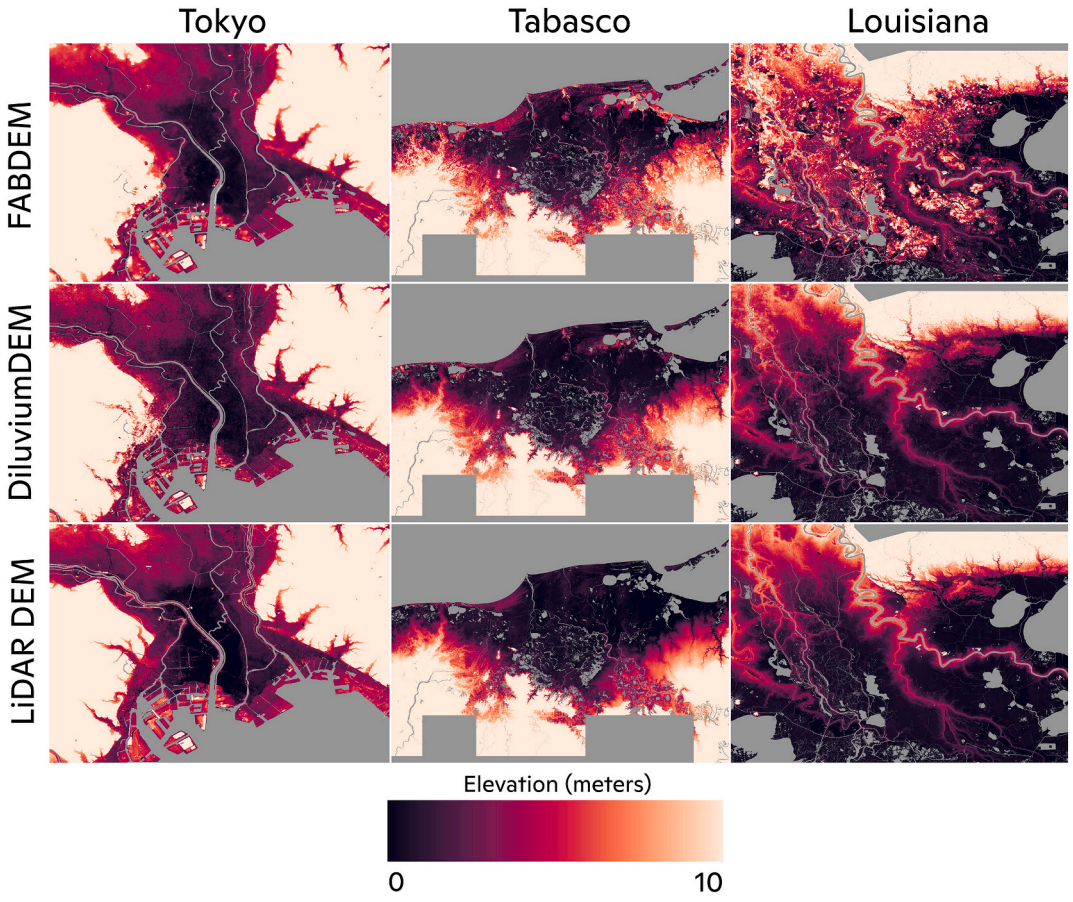

Fig. 2. Comparison of elevations in meters between FABDEM (top row), DiluviumDEM (middle row), and LiDAR-based DEM (bottom row) for three locations: Tokyo, Japan (left column), Tabasco, Mexico (center column), and southern Louisiana, USA (right column). Water pixels and areas with no LiDAR data are shown in gray.

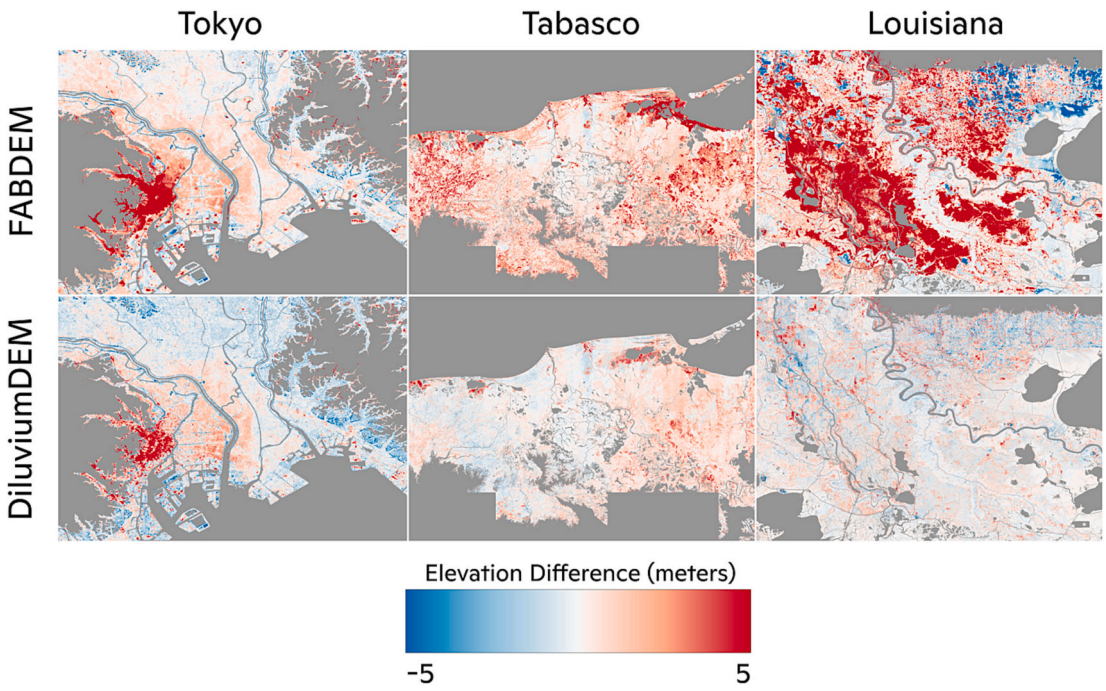

Fig. 3. The difference of elevation in meters between the global DEM and reference LiDAR DEM for FABDEM (top row) and DiluviumDEM (bottom row) for three locations: Tokyo, Japan (left column), Tabasco, Mexico (center column), and southern Louisiana, USA (right column). Water pixels, areas with no LiDAR data, and elevations greater than 20 m according to the LiDAR DEM are shown in gray.

results presented show that DiluviumDEM is generalizable across geographies and the globe.

3.3. Global validation

To estimate a global picture of the accuracy of DiluviumDEM and other commonly used coastal global DEMs, satellite LiDAR data from ICESat2 was used as reference data to calculate the RMSE and MAE of DiluviumDEM, FABDEM, and CoastalDEMV2.1 globally as shown in Table 6. ICESat2 data from June 1, 2021 to December 22, 2021 was used for this validation analysis. This time period of ICESat2 data is shorter than what was used for the ICESat2 input variable because there were approximately 2.4 million data points used from the June to December 2021 timeframe for validation. For all elevation thresholds, DiluviumDEM outperforms the other two DEMs using the RMSE and MAE metrics. This is consistent with the analysis with airborne LiDAR-derived DEMs. Additionally, this is a significant finding given that ICESat2 LiDAR data was used to train a machine learning model to create CoastalDEMV2.1. CoastalDEMV2.1 has an ME closer to zero than DiluviumDEM and FABDEM; however, the magnitude difference between the ME of DiluviumDEM and CoastalDEMV2.1 range from 2 to 25 cm. It is appropriate then that CoastalDEMV2.1 shows slightly lower error metrics than FABDEM when using ICESat2 data as the reference dataset since CoastalDEMV2.1 was trained on ICESat2 data and FABDEM was trained on airborne LiDAR-derived DEMs. The distribution of errors globally can be seen in Fig. 4 for all three DEMs. There are more points in the CoastalDEM map because the number of points that are used for each map is dependent on the DEM. We use an elevation threshold of 5 m and pixels are selected for calculation of the error metric if the DEM or the ICESat2 data shows the pixel is below 5 m. Therefore, because CoastalDEM is biased low, as shown in Table 3, there are more pixels that fall under the 5-m threshold and are then used in the creation of the map.

Table 6
RMSE and MAE in meters for different global DEMs using global ICESat2 data as the reference dataset. Only pixels with elevations greater than zero and less than the elevation threshold, according to both the LiDAR or the global DEM, were used. The value closest to zero of each row is in bold.

RMSE			
Elevation Threshold (m)	DiluviumDEM	FABDEM	CoastalDEMV2.1
2	**1.77**	2.65	2.11
5	**1.74**	2.46	2.24
10	**1.76**	2.45	2.38
MAE			
Elevation Threshold (m)	DiluviumDEM	FABDEM	CoastalDEMV2.1
2	**0.89**	1.28	1.38
5	**0.89**	1.20	1.43
10	**0.91**	1.18	1.52
ME			
Elevation Threshold (m)	DiluviumDEM	FABDEM	CoastalDEMV2.1
2	0.32	0.87	**0.29**
5	0.27	0.74	**0.02**
10	0.27	0.69	**−0.15**

CoastalDEMV2.1 performs well throughout Asia, but is less successful in Oceania, the Amazon River delta, and the Atlantic coastline of the United States. FABDEM has similar spatial patterns as CoastalDEMV2.1, but shows lower errors in western Asia and greater errors in the Amazon River delta. DiluviumDEM has the lowest RMSE across all regions with the most notable improvements in the eastern seaboard of the United States, the Gulf of Mexico, the Caribbean, and throughout Oceania. All DEMs show high errors along coastlines with steep slopes. For example, throughout Chile and Alaska all DEMs show errors mostly above 3 m.

4. Discussion

DiluviumDEM is the most accurate and precise coastal 30-m global DEM available to the public. Not only does it outperform other DEMs in areas where the machine learning model was trained, but more importantly, the ME, MAE, and RMSE of DiluviumDEM are significantly closer to zero for countries where no training data was utilized. This demonstrates the generalizability of DiluviumDEM across various regions of the world and the advantage of using DiluviumDEM compared to other coastal global DEMs. Additionally, as geodesic methods improve and

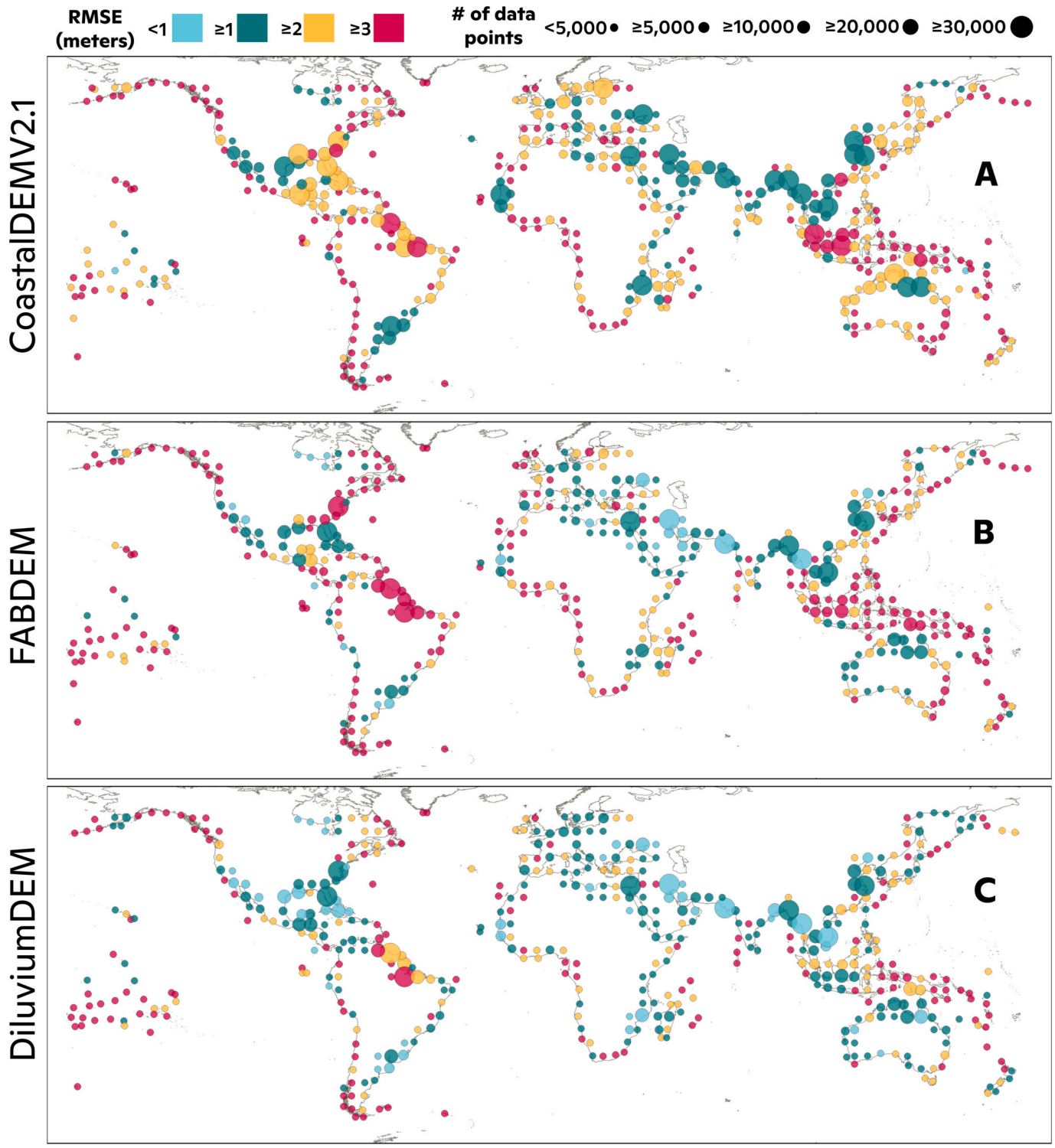

Fig. 4. Global distribution of RMSE using ICESat2 data as the reference DEM for CoastalDEMV2.1 (A), FABDEM (B), and DiluviumDEM (C). Each point represents a 5-degree cell and is represented 2-dimensionally: the size identifies how many 30-m pixels were used in the calculation and the color represents the RMSE in meters. Only pixels with elevations greater than zero and less than 5 m, according to both the ICESat2 data or the global DEM, were used.

geoids with greater precision are developed, the uncertainties due to transformations between vertical reference systems will diminish. The EGM96 geoid, used by several global DEMs such as CoastalDEMV2.1, is much less accurate than the EGM2008 geoid, used by DiluviumDEM and FABDEM. Transforming from and to EGM96 introduces more uncertainty into a DEM and consequently any inundation mapping utilizing that DEM.

While it is important to obtain a global picture of error for DEMs using ICESat2 LiDAR data, the analysis should be caveated by the fact that ICESat2 LiDAR data contains errors that reduce the efficacy of the ICESat2 data as a reference dataset. For example, it was found that in northern Australia the ICESat2 ground elevations contain a mean error of 0.28 m and a RMSE of 0.96 m when compared to an airborne LiDAR DEM (Yu et al., 2021).

Table 7
Water level above mean sea level for respective sea level rise scenarios (i.e., M-50, L-83, and SSP2), different countries, and the confidence interval for each country and respective water level. Confidence intervals that are 68% and above are in bold to represent appropriate use of the DEM in that region.

Country	SLR Scenario	Water Level	% Confidence DiluviumDEM	% Confidence FABDEM	% Confidence CoastalDEMV2.1 (90 m)
USA	M-50	2.11	**79%**	32%	41%
	L-83	2.88	**91%**	42%	54%
	SSP2	1.90	**74%**	29%	37%
NLD	M-50	3.49	**99%**	**93%**	**83%**
	L-83	4.03	**100%**	**96%**	**88%**
	SSP2	3.28	**98%**	**91%**	**80%**
AUS	M-50	2.92	64%	43%	34%
	L-83	3.80	**76%**	54%	43%
	SSP2	2.71	60%	40%	31%
England	M-50	3.55	**94%**	**86%**	58%
	L-83	4.07	**97%**	**91%**	64%
	SSP2	3.37	**92%**	**84%**	55%
Poland	M-50	1.85	66%	40%	50%
	L-83	2.40	**78%**	51%	62%
	SSP2	1.63	60%	36%	45%
Japan	M-50	2.49	55%	38%	19%
	L-83	3.48	**71%**	52%	26%
	SSP2	2.23	50%	35%	17%
France	M-50	3.29	**90%**	67%	52%
	L-83	3.88	**95%**	**75%**	60%
	SSP2	3.10	**88%**	64%	50%
Mexico	M-50	2.38	**75%**	57%	50%
	L-83	3.26	**89%**	**72%**	65%
	SSP2	2.18	**71%**	53%	47%
Latvia	M-50	1.98	53%	43%	47%
	L-83	2.53	64%	53%	57%
	SSP2	1.77	48%	39%	42%
Denmark	M-50	1.82	58%	55%	42%
	L-83	2.35	**70%**	67%	52%
	SSP2	1.61	52%	49%	37%

Using the appropriateness framework described in the methods section, we describe the confidence level of the three DEMs previously analyzed that were most unbiased (e.g., a mean error of zero), DiluviumDEM, FABDEM, and CoastalDEMV2.1, for sea level rise in 2100 in Table 7 using the RMSE of the different country DEMs for elevations less than 2 m from Table 1. We combine the estimated sea level rise from the Intergovernmental Panel on Climate Change (IPCC) 6th Assessment Report (AR6)'s SSP5–8.5 Medium Confidence 50th percentile scenario (hereafter referred to as M-50) and the water level calculated as the 1-year return period from the CoDEC dataset (Muis et al., 2020; Fox-Kemper et al., 2021). Since the CoDEC dataset is referenced to mean sea level and DiluviumDEM is referenced to EGM2008, CoDEC 1-year water levels were converted to the EGM2008 geoid using the DTU10 Mean Dynamic Ocean Topography (MDOT) (Andersen and Knudsen, 2009), similar to the methodology presented in Kirezci et al. (2020) and Muis et al. (2017). We use the DTU10 MDOT dataset as the geoid used to calculate the MDOT was EGM2008. We take the average of all CoDEC points along a country's coastline using the EEZ as boundaries. The AR6 sea level rise projections use 1995–2014 as the baseline time period which contains the majority of the years that the data for COP30DEM was taken (i.e., 2011–2015). Therefore, DiluviumDEM and AR6 align well in terms of baseline time periods and elevation measurements and are well suited to be utilized in tandem.

We focus on the SSP-8.5 scenario for several reasons. The first is that historical total cumulative carbon dioxide emissions closely agreed with those from Representative Concentration Pathway 8.5 (RCP8.5, the predecessor of SSP5–8.5) (Schwalm et al., 2020). Secondly, while the particular drivers of projected emissions under SSP5–8.5 (e.g., coal use) may not align with future policies, the emissions themselves that will drive the climate forcing may come from other sources. Thirdly, uncertainties in climate models due to climate sensitivity and climate feedback loops are still significant (e.g., permafrost processes are largely ignored in climate models) and their contributions to future warming is underrepresented. Fourth, sea level rise estimates have been trending upward as our knowledge on sea level rise processes has grown which supports the selection of a high warming scenario (Garner et al., 2018). For example, the IPCC's 5th Assessment Report (AR5), published in 2013, estimated global mean sea level would rise by a median amount of 0.71 m by 2100 relative to the 1995–2014 global mean sea level under the RCP8.5 scenario while the more recent AR6 projects a rise of 0.77 m by 2100 under SSP5–8.5 (Fox-Kemper et al., 2021). Finally, the scientific community's understanding of Antarctica's contribution to sea level rise is not robust enough to meaningfully differentiate between sea level rise projections of SSP5–8.5 and other scenarios except for SSP1–2.6 (van de Wal et al., 2022). Yet, there is only a 0.1% chance that we will follow the SSP1–2.6 scenario, a representation of keeping global average warming to 1.5 °C also known as the Paris Agreement (Vargas Zeppetello et al., 2022).

In addition to the M-50 values, we also use the 83rd percentile sea level rise values from the SSP5–8.5 Low Confidence scenario (hereafter referred to as L-83) which incorporates low likelihood-high impact (LLHI) ice sheet processes. We focus on the 83rd percentile because the global sea level rise amounts associated with the 83rd percentile is the upper-end estimate of the high-end sea level rise estimates generated by van de Wal et al. (2022) which aimed to create actionable high-end estimates for adaptation managers. The possibility of 2-m global mean sea level rise by 2100 under SSP-8.5 cannot be ruled out as the estimate is within the 90% uncertainty bound for RCP8.5 (SSP5–8.5) (Bamber et al., 2019). To provide users with greater guidance on when DiluviumDEM is appropriate for lower sea level rise scenarios, we also provide the confidence interval for SSP2–4.5 50th percentile Medium Confidence scenario (hereafter referred to as SSP2).

For M-50 and SSP2, DiluviumDEM is appropriate for five out of the ten countries, FABDEM is appropriate for two countries, and CoastalDEMV2.1 is appropriate for just one country. Under L-83, DiluviumDEM is appropriate for nine countries, FABDEM is appropriate for four countries, and CoastalDEMV2.1 is appropriate for one country. Table 7 clearly shows that the greatest confidence for inundation

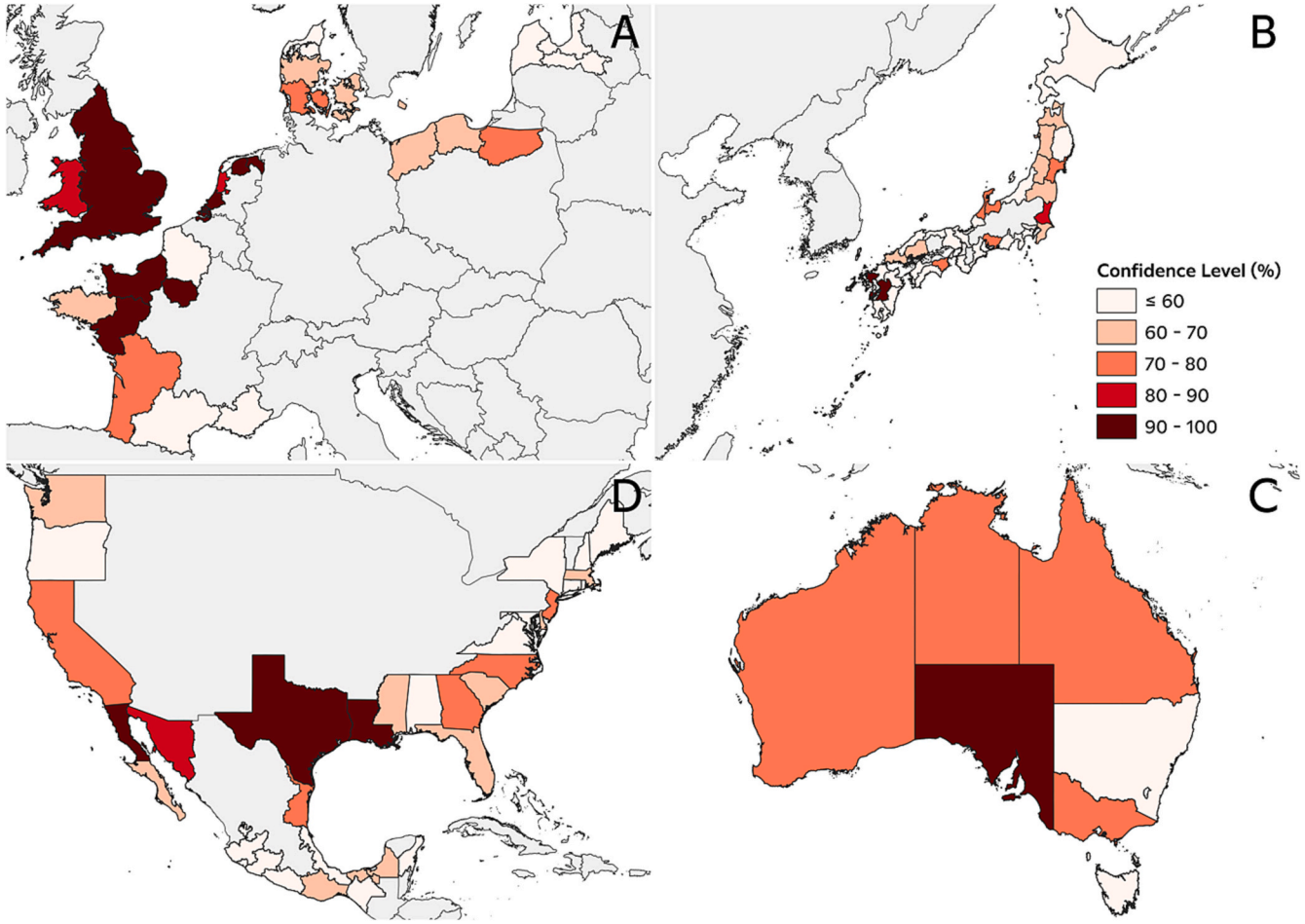

Fig. 5. DiluviumDEM M-50 scenario confidence levels for the Level 1 administrative units in (A) Europe, (B) Japan, (C) Australia, (D) North America for elevations less than 2 m above the EGM08 geoid. Administrative units in gray have either no local DEM data, no elevations below the 2-m threshold, or have no coastline.

mapping is always with DiluviumDEM and if a water level is not appropriate for mapping with DiluviumDEM, then it is not appropriate for other global DEMs.

Confidence levels also can vary within countries across Level 1 administrative units as shown in Figs. 5 and 6 for the M-50 and L-83 scenarios, respectively, for DiluviumDEM. In France there is greater confidence on the Atlantic coast compared to the Mediterranean coast which is largely a function of the 1-year water level height being higher on the Atlantic side. In the United States, confidence levels are higher in the south east and Gulf of Mexico coasts than in the Northeast due to DiluviumDEM errors being lower in the southern half of the country. It is also worth noting that while most of the states/provinces in a country can have high confidence levels, the country-wide confidence level may below the appropriateness threshold because most of the elevation values are contained in a single state or province. A good example of this is Australia where almost all the states have confidence levels of 68% or above yet the confidence level of New South Wales at 52% prevents the country-wide confidence level from reaching the appropriateness threshold of 68% for M-50.

Given the generality shown for low errors of DiluviumDEM in regions where no training data was used, we extend that assumption to flood mapping and the confidence level estimates. The practice of using global DEMs for inundation modeling in regions where global DEMs were not trained with local data and assuming error metrics from other regions where validation did occur is common (Restrepo-Ángel et al., 2021; Hoballah Jalloul et al., 2022). Still, a global measure of the confidence level for using DiluviumDEM in sea level rise inundation analysis is useful. Rather than use the error metrics based on ICESat2 reference data, we average the RMSE values in Table 1 for the ten countries because of the high relative errors for ICESat2 LiDAR measurements (Yu et al., 2021). Across the ten countries, the RMSE average is 1.13 m while the global coastal average for the M-50 scenario in addition to the 1-year water level is 2.39 m above the EGM2008 geoid, 2.20 m above the geoid for SSP2, and 3.16 m above the geoid for the L-83 percentile. These water levels correspond to a 71% confidence interval for the M-50 scenario, 67% for the SSP2 scenario, and an 84% confidence interval for the L-83 scenario. While FABDEM, the second most accurate DEM behind DiluviumDEM, is not appropriate even for the L-83 scenario with a confidence level of 63%.

While DiluviumDEM is appropriate use under the SSP5–8.5 scenario, we also argue that DiluviumDEM is appropriate for the SSP2–4.5 scenario as well given that the global average RMSE estimate is only 1 percentage point off the 68% confidence level for the 50th percentile of sea level rise. IPCC sea level rise estimates are often considered underestimates. Due to limited observational data, an incomplete understanding of ice sheet dynamics, and coarse representation of ice-ocean processes, there are significant uncertainties in how ice sheets will contribute to global sea level rise; and future estimates, including those of AR6, are likely too low (Siegert et al., 2020). Recent research has shown that sea level rise projections are largely underestimates because ice sheet models do not incorporate realistic and localized representations of ice-ocean interactions resulting in underestimating Greenland glacier mass loss by more than a factor of two (Wood et al., 2021). The committed sea-level rise contribution from Greenland is estimated to be 0.27 ± 0.68 m by 2100, equivalent to the LLHI SSP5–8.5 estimate for Greenland from van de Wal et al. (2022) for 2100 (Box et al., 2022).

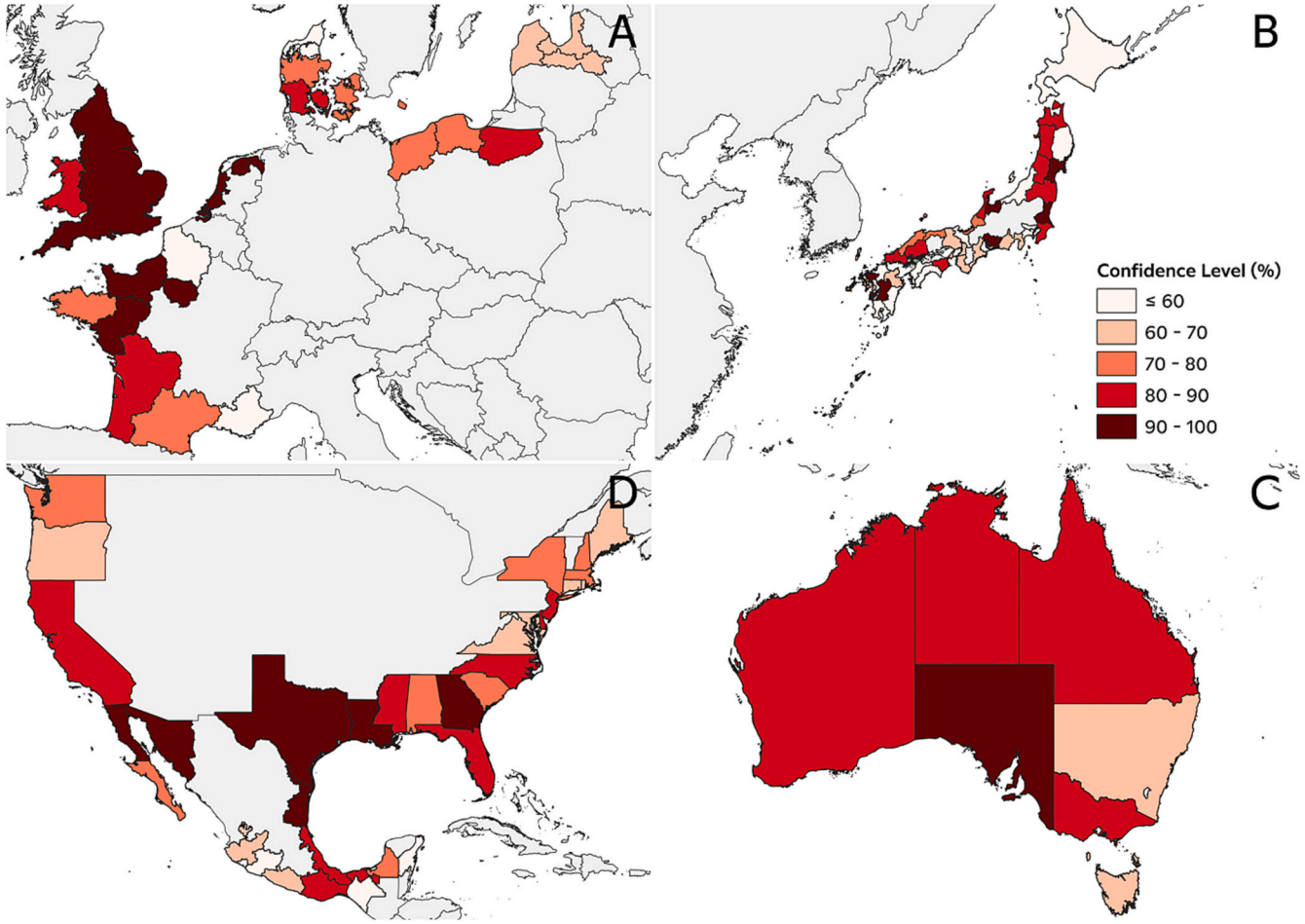

Fig. 6. DiluviumDEM L-83 scenario confidence levels for the Level 1 administrative units in (A) Europe, (B) Japan, (C) Australia, (D) North America for elevations less than 2 m above the EGM08 geoid. Administrative units in gray have either no local DEM data, no elevations below the 2-m threshold, or have no coastline.

Furthermore, sea level rise projections exclude contributions from exposed rebounding bedrock under the West Antarctic Ice Sheet and subsequent meltwater pushed oceanward increases global mean sea level by 0.01 m through 2100 (Pan et al., 2021). Additionally, new observational work on the Thwaites Glacier in West Antarctica has shown that the glacier is melting at an accelerating rate and the Thwaites Eastern Ice Shelf will likely destabilize within a few decades which increases the probability of LLHI sea level rise scenarios (Alley et al., 2021; Dos Santos et al., 2021; Wåhlin et al., 2021; Wild et al., 2022). Omitting climate variability in ice sheet model climate forcing underestimates Antarctic contribution to sea level rise by 0.07 to 0.11 m by 2100 (Tsai et al., 2020). Even the IPCC's consensus-based approach often results in lower estimates to remain conservative (Garner et al., 2018). Only one model in the AR6 sea level rise projections incorporates the Marine Ice Cliff Instability mechanism, a hypothesis that could increase sea level rise projections by decimeters (DeConto and Pollard, 2016; Edwards et al., 2021). The AR6 report acknowledges that sea level rise could reach 2.3 m by 2100 through a combination of the aforementioned processes (Fox-Kemper et al., 2021).

Due to these underestimates in the IPCC's sea level rise projections, global sea level rise by 2100 is higher than projected under SSP2 and would allow for DiluviumDEM to meet the appropriate use threshold of 68% for inundation mapping. Therefore, we present DiluviumDEM as not only a significant advancement in global coastal elevation data, but the first 30-m global DEM appropriate for sea level rise assessment through 2100 using the IPCC scenarios SSP2–4.5 and SSP5–8.5. Additionally, the use of DiluviumDEM to analyze water levels with return periods greater than 1-year would increase the confidence levels.

We caution against using DiluviumDEM for terrain analysis (such as producing a stream network) because pixels with elevations greater than 80 m in DiluviumDEM are masked. Unless the terrain analysis is coastal focused, other DEMs with higher elevation coverage are better suited for such analyses. DEMs that provide data further inland are more appropriate for terrain analysis. Further improvements to DiluviumDEM will continue as satellite data representing vegetation and building heights increase in resolution and accuracy. In Japan and England, the LightGBM model struggles in urbanized areas where building density is especially high. This is likely because commercial centers are not necessarily areas of high population density, one of the input variables, and therefore the model does not identify certain pixels that contain tall buildings and correct for this error. Additional datasets that are more representative of building height would assist in reducing the error of COP30DEM even further. High errors also persist in densely forested areas, such as in Poland, suggesting that greater fidelity is needed in forest canopy height datasets. Training the model on a greater number of LiDAR DEMs such as in Spain, New Zealand, and Argentina would also likely promote further model generalization. The constant development of new machine learning techniques will allow for further reduction in the error statistics of DiluviumDEM. Future work with DiluviumDEM will include investigating other machine learning models for elevation correction, additional accuracy metrics specific to inundation mapping, and mapping inundation extent for sea level rise globally.

5. Conclusion

As global DEMs are crucial for environmental and social analyses,

improving their accuracy is paramount as climate change progresses. For the foreseeable future, global DEMs will need to be corrected for coastal flood assessment given the lack of airborne LiDAR data for many parts of the world and that several global DEMs reference surface elevation, which includes tree canopies and building rooftops, not the underlying terrain elevation. Even the recent 2-m resolution global EarthDEM (https://www.pgc.umn.edu/data/earthdem/) is a digital surface model so the terrain is not represented.

We have presented a new global coastal DEM, DiliuviumDEM, that was created using a LightGBM regression model. Using LiDAR-based DEMs as the training dataset and 52 explanatory variables, DiluviumDEM represents an improved version of the COP30DEM dataset. DiluviumDEM shows superior accuracy across various regions, metrics, and land covers compared to other leading global DEMs. From the 90 individual comparisons (across countries, elevation thresholds, and error metrics), DiluviumDEM shows the lowest error for 70, FABDEM for 14, and CoastalDEMV2.1 for 6. In a comparison of distributions across DEMs, DiluviumDEM shows the greatest area under the curve closest to zero, emphasizing how DiluviumDEM contains the lowest errors.

The superiority of DiluviuDEM across error metrics also extends into comparing DEMs for appropriateness for sea level rise inundation mapping. Using the 68% confidence threshold as the definition for appropriate, we find that DiluviumDEM is appropriate for 50% of the countries analyzed, FABDEM is appropriate for 20%, and CoastalDEMV2.1 is appropriate for just 1% using IPCC scenarios SSP2–4.5 and SSP5–8.5. Under a low-likelihood high impact scenario, DiluviumDEM is appropriate for 90% of the countries, FABDEM is appropriate for 40%, and CoastalDEMV2.1 is appropriate for 1%. Using the composite RMSE of the assessed countries, we find that DiluviumDEM is appropriate for use globally under the SSP2–4.5 and SSP5–8.5 scenarios.

Author contributions

D.D. and C.R.S. participated in the project design. D.D. preformed the data processing, model training, and analysis of results. D.D. wrote the paper with contributions from C.R.S. and Z.Z.

Funding

This research was funded by the Woodwell Climate Research Center.

Submission declaration

This paper has not been published or submitted elsewhere and is not under consideration at another journal. All authors approve the publication of this paper. This paper will not be published elsewhere in the same form.

Current publicly available global digital elevation models (DEMs) contain high vertical errors (i.e., greater than a root mean square error of 1.75 m) that prohibit mapping sea level rise with high confidence. This lack of appropriate elevation data limits adaptation decisions where local, highly accurate elevation data is not available. The objective of this work is to create a new open access global coastal digital elevation model with lower errors than other publicly available global digital elevation models.

Declaration of Competing Interest

The authors declare that they have no known competing financial interests or personal relationships that could have appeared to influence the work reported in this paper.

Data availability

DiluviumDEM is available for download at the following Zenodo repository: https://doi.org/10.5281/zenodo.8329293 and as an Earth Engine public asset: https://code.earthengine.google.com/?asset=users/ddusseau/DiluviumDEM.

The code used to generate DiluviumDEM is available at the Github repository: https://github.com/ddusseau/DiluviumDEM.

Appendix A. Supplementary data

Supplementary data to this article can be found online at https://doi.org/10.1016/j.rse.2023.113812.

References

Airbus, July 2018. WorldDEM Technical Product Specification Digital Surface Model, Digital Terrain Model Version 2.4.

Alley, K.E., Wild, C.T., Luckman, A., Scambos, T.A., Truffer, M., Pettit, E.C., Muto, A., Wallin, B., Klinger, M., Sutterley, T., Child, S.F., 2021. Two decades of dynamic change and progressive destabilization on the Thwaites Eastern Ice Shelf. Cryosphere 15 (11), 5187–5203.

Andersen, O.B., Knudsen, P., 2009. The DNSC08 mean sea surface and mean dynamic topography. J. Geophys. Res. 114, C11.

Bamber, J.L., Oppenheimer, M., Kopp, R.E., Aspinall, W.P., Cooke, R.M., 2019. Ice sheet contributions to future sea-level rise from structured expert judgment. Proc. Natl. Acad. Sci. 116 (23), 11195–11200.

Belgiu, M., Drăguţ, L., 2016. Random forest in remote sensing: a review of applications and future directions. ISPRS J. Photogramm. Remote Sens. 114, 24–31.

Box, J.E., Hubbard, A., Bahr, D.B., Colgan, W.T., Fettweis, X., Mankoff, K.D., Wehrlé, A., Noël, B., Van Den Broeke, M.R., Wouters, B., Bjørk, A.A., 2022. Greenland ice sheet climate disequilibrium and committed sea-level rise. Nat. Clim. Chang. 12 (9), 808–813.

Chen, T., Guestrin, C., 2016, August. Xgboost: a scalable tree boosting system. In: Proceedings of the 22nd ACM Sigkdd International Conference on Knowledge Discovery and Data Mining, pp. 785–794.

Crippen, R., Buckley, S., Belz, E., Gurrola, E., Hensley, S., Kobrick, M., Lavalle, M., Martin, J., Neumann, M., Nguyen, Q., Rosen, P., 2016. NASADEM Global Elevation Model: Methods and Progress.

DeConto, R.M., Pollard, D., 2016. Contribution of Antarctica to past and future sea-level rise. Nature 531 (7596), 591–597.

Dos Santos, T.D., Barnes, J.M., Goldberg, D.N., Gudmundsson, G.H., Morlighem, M., 2021. Drivers of change of Thwaites glacier, West Antarctica, between 1995 and 2015. Geophys. Res. Lett. 48 (20) p.e2021GL093102.

Edwards, T.L., Nowicki, S., Marzeion, B., Hock, R., Goelzer, H., Seroussi, H., Jourdain, N. C., Slater, D.A., Turner, F.E., Smith, C.J., McKenna, C.M., 2021. Projected land ice contributions to twenty-first-century sea level rise. Nature 593 (7857), 74–82.

European Space Agency (ESA), 2021. Sinergise. Copernicus Global Digital Elevation Model. https://doi.org/10.5270/ESA-c5d3d65.

Fahrland, E., Paschko, H., Jacob, P., Kahabka, H., 2022. Copernicus Digital Elevation Model Product Handbook. European Space Agency, Airbus.

Farr, T.G., Rosen, P.A., Caro, E., Crippen, R., Duren, R., Hensley, S., Alsdorf, D., 2007. The shuttle radar topography mission. Rev. Geophys. 45 (2).

Flanders Marine Institute, 2020. Union of the ESRI Country Shapefile and the Exclusive Economic Zones (version 3). https://doi.org/10.14284/403. Available online at. https://www.marineregions.org/.

Fox-Kemper, B., Hewitt, H.T., Xiao, C., Aðalgeirsdóttir, G., Drijfhout, S.S., Edwards, T.L., Golledge, N.R., Hemer, M., Kopp, R.E., Krinner, G., Mix, A., Notz, D., Nowicki, S., Nurhati, I.S., Ruiz, L., Sallée, J.-B., Slangen, A.B.A., Yu, Y., 2021. Ocean, cryosphere and sea level change. In: Masson-Delmotte, V., Zhai, P., Pirani, A., Connors, S.L., Péan, C., Berger, S., Caud, N., Chen, Y., Goldfarb, L., Gomis, M.I., Huang, M., Leitzell, K., Lonnoy, E., Matthews, J.B.R., Maycock, T.K., Waterfield, T., Yelekçi, O., Yu, R., Zhou, B. (Eds.), Climate Change 2021: The Physical Science Basis. Contribution of Working Group I to the Sixth Assessment Report of the Intergovernmental Panel on Climate Change. Cambridge University Press, Cambridge, United Kingdom and New York, NY, USA, pp. 1211–1362. https://doi.org/10.1017/9781009157896.011.

Gallant, J.C., Read, A., 2009. Enhancing the SRTM data for Australia. Proc. Geomorphom. 31, 149–154.

Garner, A.J., Weiss, J.L., Parris, A., Kopp, R.E., Horton, R.M., Overpeck, J.T., Horton, B. P., 2018. Evolution of 21st century sea level rise projections. Earth's Future 6 (11), 1603–1615.

Gesch, D.B., 2018. Best practices for elevation-based assessments of sea-level rise and coastal flooding exposure. Front. Earth Sci. 6, 230.

Gesch, D., 2023. Assessing Global Elevation Models for Mapping the Low Elevation Coastal Zone. In: Geomorphometry, 2023.

Gorelick, N., Hancher, M., Dixon, M., Ilyushchenko, S., Thau, D., Moore, R., 2017. Google earth engine: planetary-scale geospatial analysis for everyone. Remote Sens. Environ. 202, 18–27.

Guth, Peter L., Geoffroy, Tera M., 2021. LiDAR point cloud and ICESat-2 evaluation of 1 second global digital elevation models: Copernicus wins. Transactions in GIS 25 (5), 2245–2261.

Hawker, L., Neal, J., Bates, P., 2019. Accuracy assessment of the TanDEM-X 90 digital elevation model for selected floodplain sites. Remote Sens. Environ. 232, 111319.

Hawker, L., Uhe, P., Paulo, L., Sosa, J., Savage, J., Sampson, C., Neal, J., 2022. A 30 m global map of elevation with forests and buildings removed. Environ. Res. Lett. 17 (2), 024016.
Hoballah Jalloul, M., Scheiber, L., Jordan, C., Visscher, J., Nguyen, H.Q., Schlurmann, T., 2022. Uncovering inundation hotspots through a normalized flood severity index: urban flood modelling based on open-access data in Ho Chi Minh City, Vietnam. Nat. Hazards Earth Syst. Sci. Discuss. 1–33.
Inter-Governmental Committee on Surveying and Mapping (ICSM), 2008. ICSM Guidelines for Digital Elevation Data. https://icsm.gov.au/sites/default/files/2017-03/ICSM-GuidelinesDigitalElevationDataV1.pdf.
Karra, K., Kontgis, C., Statman-Weil, Z., Mazzariello, J.C., Mathis, M., Brumby, S.P., 2021, July. Global land use/land cover with sentinel 2 and deep learning. In: In 2021 IEEE International Geoscience and Remote Sensing Symposium IGARSS. IEEE, pp. 4704–4707.
Ke, G., Meng, Q., Finley, T., Wang, T., Chen, W., Ma, W., Ye, Q., Liu, T.Y., 2017. Lightgbm: a highly efficient gradient boosting decision tree. Adv. Neural Inf. Proces. Syst. 30.
Khasanov, K., 2020, July. Evaluation of ASTER DEM and SRTM DEM data for determining the area and volume of the water reservoir. In: IOP Conference Series: Materials Science and Engineering, vol. 883. IOP Publishing, p. 012063. No. 1.
Kirezci, E., Young, I.R., Ranasinghe, R., Muis, S., Nicholls, R.J., Lincke, D., Hinkel, J., 2020. Projections of global-scale extreme sea levels and resulting episodic coastal flooding over the 21st century. Sci. Rep. 10 (1), 1–12.
Kulp, S.A., Strauss, B.H., 2018. CoastalDEM: a global coastal digital elevation model improved from SRTM using a neural network. Remote Sens. Environ. 206, 231–239.
Kulp, S.A., Strauss, B.H., 2021. CoastalDEM v2. 1: a high-accuracy and high-resolution global coastal elevation model trained on ICESat-2 satellite lidar.
Lesparre, J., Huisman, L., Alberts, B., 2020. Nederlandse Samenwerking Geodetische Infrastructuur. RDNAPTRANS2018: Coordinate transformation to and from Stelsel van de Rijksdriehoeksmeting and Normaal Amsterdams Peil.
Li, Y., Fu, H., Zhu, J., Wu, K., Yang, P., Wang, L., Gao, S., 2022. A method for SRTM DEM elevation error correction in forested areas using ICESat-2 data and vegetation classification data. Remote Sens. 14 (14), 3380.
Muis, S., Verlaan, M., Nicholls, R.J., Brown, S., Hinkel, J., Lincke, D., Vafeidis, A.T., Scussolini, P., Winsemius, H.C., Ward, P.J., 2017. A comparison of two global datasets of extreme sea levels and resulting flood exposure. Earth's Future 5 (4), 379–392.
Muis, S., Apecechea, M.I., Dullaart, J., de Lima Rego, J., Madsen, K.S., Su, J., Yan, K., Verlaan, M., 2020. A high-resolution global dataset of extreme sea levels, tides, and storm surges, including future projections. Front. Mar. Sci. 7, 263.
Myers, E., Hess, K., Yang, Z., Xu, J., Wong, A., Doyle, D., Woolard, J., White, S., Le, B., Gill, S., Hovis, G., 2007. VDatum and strategies for national coverage. In: OCEANS 2007. IEEE, pp. 1–8.
National Oceanic and Atmospheric Administration [NOAA], 2010. Technical considerations for use of geospatial data in sea level change mapping and assessment. In: NOAA Technical Report NOS 2010-01. NOAA, Silver Spring, MD.
National Oceanic and Atmospheric Administration (NOAA), 2012. Lidar 101: An Introduction to Lidar Technology, Data, and Applications.
National Oceanic and Atmospheric Administration (NOAA), 8 Nov. 2021. NOAA/Nos Vertical Datums Transformation. NOAA/NOS's VDatum, US Department of Commerce. https://vdatum.noaa.gov/docs/est_uncertainties.html#estTransform. Allen.
Pan, L., Powell, E.M., Latychev, K., Mitrovica, J.X., Creveling, J.R., Gomez, N., Hoggard, M.J., Clark, P.U., 2021. Rapid postglacial rebound amplifies global sea level rise following West Antarctic ice sheet collapse. Sci. Adv. 7 (18) p.eabf7787.
Pavlis, N.K., Holmes, S.A., Kenyon, S.C., Factor, J.K., 2012. The development and evaluation of the Earth Gravitational Model 2008 (EGM2008). J. Geophys. Res. Solid Earth 117 (B4).
Pham, T.D., Le, N.N., Ha, N.T., Nguyen, L.V., Xia, J., Yokoya, N., To, T.T., Trinh, H.X., Kieu, L.Q., Takeuchi, W., 2020. Estimating mangrove above-ground biomass using extreme gradient boosting decision trees algorithm with fused sentinel-2 and ALOS-2 PALSAR-2 data in can Gio biosphere reserve, Vietnam. Remote Sens. 12 (5), 777.
Rabus, B., Eineder, M., Roth, A., Bamler, R., 2003. The shuttle radar topography mission—a new class of digital elevation models acquired by spaceborne radar. ISPRS J. Photogramm. Remote Sens. 57 (4), 241–262.
Restrepo-Ángel, J.D., Mora-Páez, H., Díaz, F., Govorcin, M., Wdowinski, S., Giraldo-Londoño, L., Tosic, M., Fernández, I., Paniagua-Arroyave, J.F., Duque-Trujillo, J.F., 2021. Coastal subsidence increases vulnerability to sea level rise over twenty first century in Cartagena, Caribbean Colombia. Sci. Rep. 11 (1), 1–13.
Santillan, J.R., Makinano-Santillan, M., 2016. Vertical Accuracy Assessment of 30-M Resolution Alos, Aster, and Srtm Global Dems over Northeastern Mindanao, Philippines. International Archives of the Photogrammetry, Remote Sensing & Spatial Information Sciences, p. 41.
Schwalm, C.R., Glendon, S., Duffy, P.B., 2020. RCP8. 5 tracks cumulative CO2 emissions. Proc. Natl. Acad. Sci. 117 (33), 19656–19657.
Siegert, M., Alley, R.B., Rignot, E., Englander, J., Corell, R., 2020. Twenty-first century sea-level rise could exceed IPCC projections for strong-warming futures. One Earth 3 (6), 691–703.
Tadono, T., Ishida, H., Oda, F., Naito, S., Minakawa, K., Iwamoto, H., 2014. Precise global DEM generation by ALOS PRISM. ISPRS Ann. Photogramm. Remote Sens. Spat. Inform. Sci. 2 (4), 71.
Tsai, C.Y., Forest, C.E., Pollard, D., 2020. The role of internal climate variability in projecting Antarctica's contribution to future sea-level rise. Clim. Dyn. 55 (7), 1875–1892.
Tyree, S., Weinberger, K.Q., Agrawal, K., Paykin, J., 2011, March. Parallel boosted regression trees for web search ranking. In: Proceedings of the 20th International Conference on World Wide Web, pp. 387–396.
Vargas Zeppetello, L.R., Raftery, A.E., Battisti, D.S., 2022. Probabilistic projections of increased heat stress driven by climate change. Commun. Earth Environ. 3 (1), 1–7.
Vernimmen, R., Hooijer, A., Pronk, M., 2020. New ICESat-2 satellite LiDAR data allow first global lowland DTM suitable for accurate coastal flood risk assessment. Remote Sens. 12 (17), 2827.
Wåhlin, A.K., Graham, A.G.C., Hogan, K.A., Queste, B.Y., Boehme, L., Larter, R.D., Pettit, E.C., Wellner, J., Heywood, K.J., 2021. Pathways and modification of warm water flowing beneath Thwaites ice shelf, West Antarctica. Sci. Adv. 7 (15) p. eabd7254.
van de Wal, R.S., Nicholls, R.J., Behar, D., McInnes, K., Stammer, D., Lowe, J.A., Church, J.A., DeConto, R., Fettweis, X., Goelzer, H., Haasnoot, M., 2022. A high-end estimate of sea level rise for practitioners. Earth's Future 10 (11) p.e2022EF002751.
Wild, C.T., Alley, K.E., Muto, A., Truffer, M., Scambos, T.A., Pettit, E.C., 2022. Weakening of the pinning point buttressing Thwaites Glacier, West Antarctica. Cryosphere 16 (2), 397–417.
Wood, M., Rignot, E., Fenty, I., An, L., Bjørk, A., van den Broeke, M., Cai, C., Kane, E., Menemenlis, D., Millan, R., Morlighem, M., 2021. Ocean forcing drives glacier retreat in Greenland. Sci. Adv. 7 (1) p.eaba7282.
Woodruff, S., BenDor, T.K., 2018. GIS and Coastal Vulnerability to Climate Change.
Yu, J., Nie, S., Liu, W., Zhu, X., Lu, D., Wu, W., Sun, Y., 2021. Accuracy assessment of ICESat-2 ground elevation and canopy height estimates in mangroves. IEEE Geosci. Remote Sens. Lett. 19, 1–5.
Zhang, K., Gann, D., Ross, M., Robertson, Q., Sarmiento, J., Santana, S., Fritz, C., 2019. Accuracy assessment of ASTER, SRTM, ALOS, and TDX DEMs for Hispaniola and implications for mapping vulnerability to coastal flooding. Remote Sens. Environ. 225, 290–306.